Ultra-Low-Loss Slow-Light Thin-Film Lithium Niobate Optical Modulator

*Chenlei Li, Jianghao He, Ming Zhang, Yeyu Tong, Weixi Liu, Siyuan Wang, Lijia Song, Hongxuan Liu, Hengzhen Cao, Liu Liu, Yaocheng Shi, and Daoxin Dai**

Electro-optic modulators for next-generation optical interconnects require low loss-efficiency products ($\alpha V_\pi L$), compact footprints, high modulation efficiency and broad bandwidths. Here it is proposed and demonstrated a low-loss high-efficiency thin-film lithium niobate Mach–Zehnder modulator enabled by a novel ultralow-loss slow-light structure based on apodized gratings in cascade. The present loss-engineered slow-light structure achieves excess losses as low as 0.6 dB mm^{-1} experimentally, which is tens of times lower than conventional slow-light structures, and a high modulation bandwidth up to 320 GHz in theory is achieved with optimally-designed capacitively-loaded traveling-wave electrodes. Experimentally, the fabricated slow-light modulator with a 2.8-mm-long modulation region has an ultra-low loss-efficiency product $\alpha V_\pi L$ of 7.4 V dB and a flat electro-optic response up to 67 GHz, enabling 100-Gbps on-off keying with high ERs of 4.5 dB at a low driving voltage of 2V_{pp}, while 200-Gbps PAM4 and 150-Gbps PAM8 signals are also generated to show great promise for advanced modulation formats. In particular, it has also achieved the highest figure-of-merit (FOM = BR×(ER/V_{pp})/($V_\pi L$)) of ≈182 Gbps•(dB/V)/(V•cm) for high-speed optical modulation. The outstanding performance of the present slow-light modulator shows great potential and paves the way for developing high-speed optical interconnects for both data-centers and high-performance computing systems.

1. Introduction

The relentless growth of data traffic is driving the need for optical interconnects with unprecedented capacity and efficiency.[1–5] To keep pace with this demand, optical interconnects are moving toward Terabit-per-second scale throughput on a single chip. Meeting these requirements calls for ideal electro-optic (EO) modulators with low loss-efficiency products ($\alpha V_\pi L$), compact footprints, high modulation efficiencies, low propagation losses, and broad bandwidths.[2] Such high-performance modulators are crucial for various applications, including data centers, co-packaged optics, and computercom. Among various EO modulation approaches,[6–15] thin-film lithium niobate (TFLN) has established itself as a superior candidate for next-generation modulators, combining low propagation loss and excellent inherent Pockels effect[15–29] However, lithium niobate still has a relatively low EO coefficient of γ_{33}≈27 pm V^{-1}, which is much lower than, e.g., EO polymer with a high EO coefficient of 170 pm V^{-1},[30] and thus limits the modulation efficiency (V_πL) to 2.2–2.8 V cm.[15] As a result, TFLN modulators typically require device lengths of 10–20 mm to achieve low drive voltages,[28] leading to increased microwave attenuation and eventually compromising the electro-optic bandwidth. For example, the work in ref. [15] reported LN Mach-Zehnder modulators (MZMs) with a device length of 5 mm achieved a bandwidth of ≈100 GHz. However, when the device length was extended to 20 mm, the bandwidth significantly decreased to ≈45 GHz.

Various approaches have been explored to enhance the modulation efficiency and reduce the device footprint, including microring resonators,[20] photonic crystals (PhC) cavities,[21,31] Fabry-Pérot (FP) cavities,[18,22] slow-light waveguides,[23,32–36] etc. More details for the performances of these optical modulators are given in Table S1 (Supporting Information). Among them, slow-light modulators are particularly promising as they can significantly enhance the interaction between the optical field and the modulating electric field by slowing the group velocity.[37–41] However, conventional slow-light waveguides based on, e.g., photonic crystals, usually suffer from inherent drawbacks. They

C. Li, J. He, M. Zhang, W. Liu, S. Wang, L. Song, H. Liu, H. Cao, L. Liu, Y. Shi, D. Dai
State Key Laboratory for Extreme Photonics and Instrumentation, College of Optical Science and Engineering, International Research Center for Advanced Photonics
Zhejiang University
Zijingang Campus, Hangzhou 310058, China
E-mail: dxdai@zju.edu.cn

Y. Tong
Microelectronics Thrust
The Hong Kong University of Science and Technology
Guangzhou 510000, China

D. Dai
Jiaxing Key Laboratory of Photonic Sensing & Intelligent Imaging, Intelligent Optics & Photonics Research Center, Jiaxing Research Institute
Zhejiang University
Jiaxing 314000, China

The ORCID identification number(s) for the author(s) of this article can be found under https://doi.org/10.1002/lpor.202401998

DOI: 10.1002/lpor.202401998

typically exhibit strong wavelength dependence, as the strong slow-light effect is restricted to the band edges. More importantly, the increased light-matter interaction in these structures often leads to excessive propagation losses, limiting the achievable bandwidth and efficiency for modulation. For example, in ref. [35], when the enhancement factor for the group index of the slow-light structure increases from 2.4 to 5.5, the optical propagation loss significantly increases from 1.9 dB to more than 20 dB, and the E-O bandwidth greatly drops from 24.9 to 10 GHz. Recently a SiN-loaded TFLN modulator was achieved with impressive efficiency $V_\pi \cdot L$ of 0.21 V·cm and a bandwidth as large as ≥110 GHz by using topological slow-light waveguides.[42] One should notice that those devices were designed with small feature sizes of 80 nm and exhibited strong wavelength dependence. When increasing $V\pi \cdot L$ from 2.2 to 0.21, the corresponding excess loss significantly increases from 5 dB to ≥15 dB, as estimated from the reported data in ref. [42].

Alternatively, slow-light modulators based on uniform gratings in the cascade were proposed with flat-top spectral responses and simplified designs.[23,32,43,44] Recent demonstrations of slow-light MZMs on silicon[32] and TFLN [23] have shown impressive performance with high bandwidths (>110 GHz or ≈50 GHz) and low V_πL values (0.96 or 1.29 V cm). However, these devices still require high drive voltages (5 V_{pp} for silicon[32] or 8.5 V_{pp} for TFLN[23]) even for achieving relatively low extinction ratios of 2 or 3.1 dB, as the length of the modulation region is not allowed to be extended to the millimeter-scale due to the very high substantial propagation loss of 5.4 dB mm^{-1} for silicon or 13.3 dB mm^{-1} for TFLN. Therefore, it is still very challenging to make slow-light MZMs excel in all the key properties, such as low losses, compact footprints, low driving voltages, and particularly high bandwidths.

In this work, we propose and experimentally demonstrate a novel slow-light modulator architecture offering high electro-optic bandwidth far exceeding 67 GHz with ultra-low propagation loss of 0.6 dB mm^{-1}, realized by introducing a unique design based on apodized gratings (instead of conventional uniform gratings). In this way, the grating is apodized gradually, and thus, the mode-mismatch loss is significantly reduced. Furthermore, the optical field in the grating is enhanced well in the regions with the shallowest grating corrugation, which greatly alleviates the light interaction with the grating corrugation during the light propagation, thus significantly reducing the scattering loss. Besides, the high modulation bandwidth has been achieved by optimizing capacitively loaded traveling-wave electrodes (CLTW), enabling effective velocity and impedance matching between the RF and optical signals. For the fabricated slow-light MZM designed with an extended device length of 2.8 mm and $V_\pi L$ of 1.23 V cm, a loss-efficiency product αV_πL as low as 7.4 dB V is achieved as the best one for slow-light modulators, to the best of our knowledge. $V_\pi L$ is widely used for evaluating the modulation efficiency of electro-optic modulators. However, optical loss is a critical factor for slow-light modulators due to the enhanced light-matter interaction, which often leads to significantly increased propagation loss α. Thus, we combine them for slow-light modulators to provide a more comprehensive performance metric to optimally balance both optical and electrical performances.[2] Finally, we successfully demonstrate high-speed data transmissions with the data rate of 100 Gbps (OOK), 200 Gbps (PAM-4), and 150 Gbps (PAM-8), showing decent dynamic extinction ratios of 4.5, 3.8, and 3.6 dB even with a peak-to-peak voltage V_{pp} of only 2.0 V. To comprehensively evaluate optical modulators which are always desired to have high bit rates (BRs), high extinction ratios (ERs) normalized with respective to V_{pp} and low V_πL (high modulation efficiency), here we define a special figure-of-merit (FOM) as BR×(ER/V_{pp})/(V_πL), and the present slow-light modulator has a FOM of ≈182 Gbps•(dB/V)/(V•cm), which is the highest among all reported optical modulators. The outstanding performance of the present apodized-grating-based slow-light MZM shows great potential and paves the way for developing high-speed optical interconnects available for both data centers and high-performance computing systems.

2. Structure and Design

The modulation efficiency $V_\pi L$ of a TFLN slow-light MZM with a push-pull configuration is given as[32]:

$$V_\pi L = \frac{\lambda \cdot g}{2 \cdot \Gamma \cdot n_g \cdot n^2 \cdot \gamma_{33}} \tag{1}$$

where λ is the wavelength, n is the refractive index, γ_{33} is the EO coefficient, and g is the electrode gap, Γ represents the EO overlap factor of the optical mode, n_g is the group index. Considering the limitation posed by reducing the electrode spacing on the modulation-efficiency improvement, enhancing the n_g is an effective approach to improve the modulation efficiency. However, slow-light waveguides based on conventional uniform gratings suffer from significant scattering losses as well as mode-mismatch losses, limiting the allowable interaction length and, consequently, the achievable dynamic extinction ratio (ER).[23,32] The high loss in conventional slow-light waveguides is attributed to two main factors [45–50]: One is the enhanced optical scattering loss due to light interaction with the grating corrugation during the light propagation, especially near the π-phase-shift regions. The other one is the mode mismatch loss between the grating and non-grating sections. Addressing these loss mechanisms is essential for realizing efficient, low-drive-voltage, slow-light modulators with extended interaction lengths and improved performance.

To overcome these limitations, we leverage an ultralow-loss slow-light waveguide architecture to achieve an electro-optic (EO) modulator with low-loss-efficiency products (αV_πL), compact footprints, high modulation efficiencies, low propagation losses, and broad bandwidths, as shown in **Figure 1a–d**. For the present slow-light waveguide, two adjacent apodized gratings are separated by a π-phase shift to form a resonator, as shown in Figure 1b. The number of cascaded resonators is denoted by N_p. The apodized-grating corrugation depth δ is defined by the following Gaussian function [51,52] to achieve a gradual change in the mode field within the slow light waveguide,

$$\delta = \delta_0 \exp\left[-b\left(\frac{i}{N} - \frac{1}{2}\right)^2\right] \tag{2}$$

where δ_0 is the offset maximum, b is the apodization strength, and N is the number of grating teeth. The width for the central

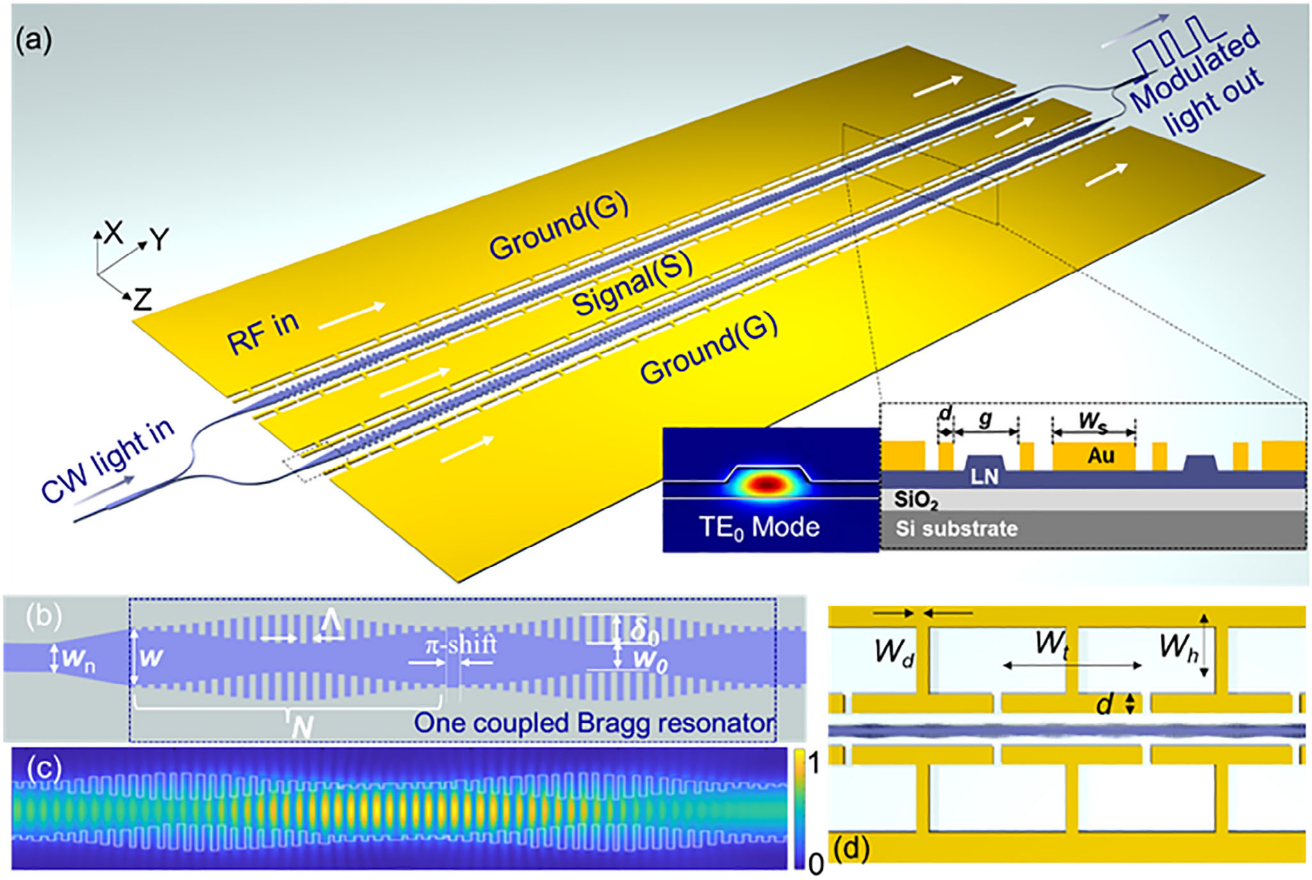

Figure 1. a) Schematic configuration of the proposed slow-light modulator. Inset: left, simulated mode profile in the designed LN photonic waveguide; right, cross-sectional schematic of the nanophotonic LN modulator. b) Top view of the coupled Bragg resonator-based slow-light waveguide that consists of a series of Bragg-gratings separated by a π-phase shift region, and the transition part connected to the normal waveguide, with the width of normal waveguide $W_n = 1$ µm, to the width of end of Bragg-gratings $W = 1.2$ µm, with a taper length $L_{tp} = 5$ µm. c) Simulated light propagation in the designed slow-light waveguide. d) Schematic view of the proposed periodic capacitively loaded traveling-wave (CLTW) electrode structure.

part of the waveguide is w_0. Our simulation reveals that the optical field is strongly localized and enhanced in the low-loss π-phase-shift regions (Figure 1c), as discussed before.[53]

This gradual grating apodization significantly reduces the mode-mismatch losses during propagation, particularly as the optical field enhancement in the π-phase-shift regions, where the grating corrugation is the shallowest and light interaction with the grating corrugations is substantially mitigated. Moreover, the π-phase-shift region features a relatively wider waveguide core compared to other sections of the slow-light waveguides. Based on our previous work,[54] for the loss introduced by the nonuniformity of the refractive index due to the sidewall roughness, the transmission loss decreases as the waveguide core width increases. Consequently, the interaction of the enhanced field with the waveguide surface is substantially decreased, effectively reducing the scattering loss of the slow-light waveguide. Additionally, the present design with apodized gratings also elegantly minimizes the mode mismatch between the slow-light waveguides and the regular waveguides. As shown in Figure 1b, the transition from a standard waveguide width of $W_n = 1$ µm to a Bragg grating region of $W = 1.2$ µm is facilitated by a tapered section with a length of $L_{tp} = 5$ µm, which is sufficient to enable adiabatic mode evolution. In contrast, conventional uniform gratings introduce abrupt transitions, resulting in additional mode mismatch losses (see more details in Notes S1 and S2, Supporting Information). It should be noted that the present mode's gradient resulting from the intrinsic apodization in the slow-light waveguide differs from the approach described in ref. [33], where an additional linear taper was introduced to reduce mode mismatch, it inadvertently acted as an additional reflector at both ends of the slow light waveguide, thereby inducing excess loss. In contrast, our design strategy significantly reduces the scattering losses, facilitating efficient electro-optic modulation without excessive propagation losses.

The proposed slow-light waveguides are designed with a 400 nm-thick X-cut LN thin film in this work, an air upper-cladding, and a 3-µm-thick SiO_2 under-cladding layer, while the ridge height is designed to be 200 nm. The mode profile of the TE_0 mode in the designed LN photonic waveguide is shown by the inset in Figure 1a (left). The designed slow-light MZM works with the push-pull configuration, and the cross-section of the modulation region is given by the inset in Figure 1a (right).

To further understand the effect of the proposed slow-light waveguide on performance improvement, we investigate the key

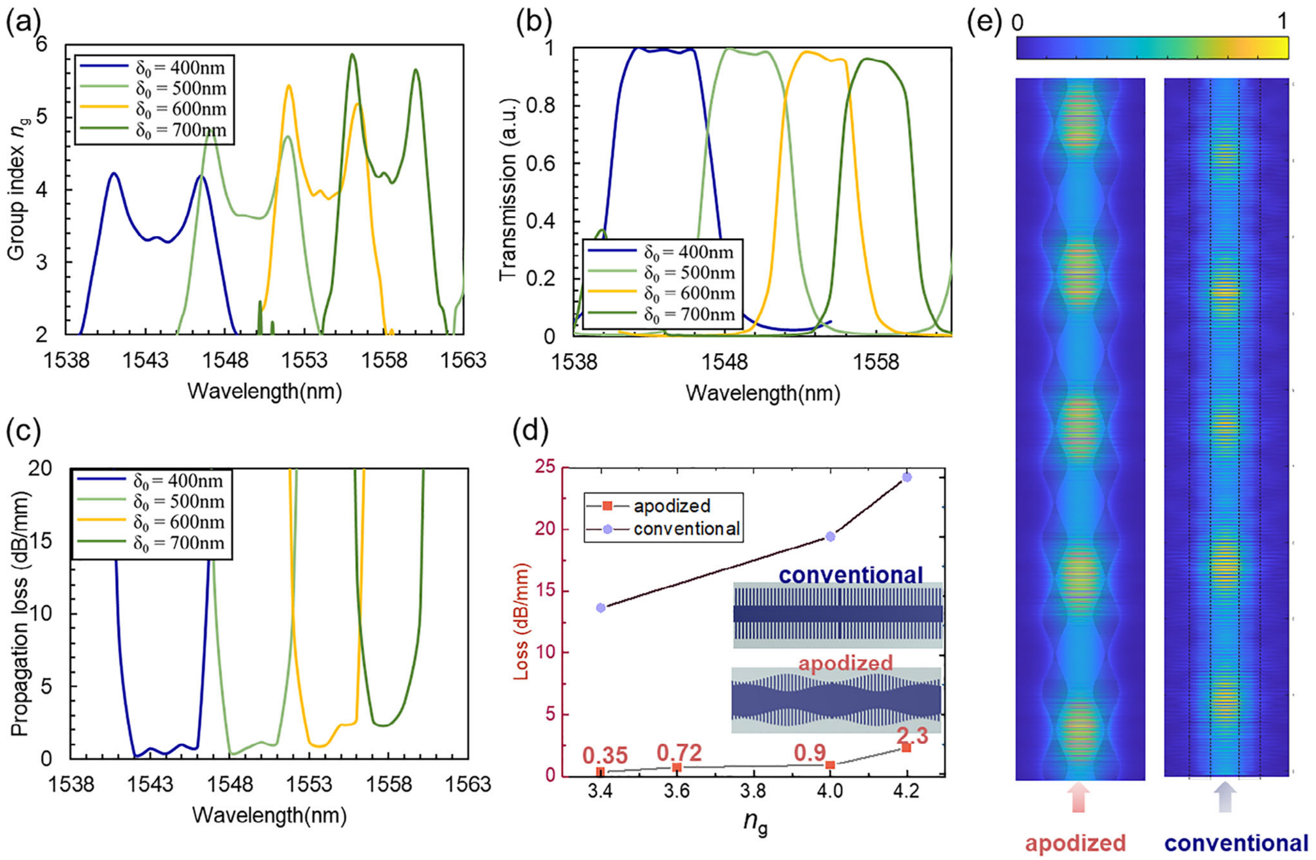

Figure 2. Calculated results of the apodized-grating slow-light waveguide: a) group index n_g. b) transmission spectral responses. c) calculated propagation loss. d) calculated losses for the apodized-grating and conventional slow-light waveguide. e) Simulated electric field intensity distributions inside the apodized-grating and conventional slow-light waveguides with $n_g \approx 4.2$.

properties of the structure. **Figure** 2a–c presents the calculated group index n_g, transmission spectral, and propagation loss for the proposed slow-light waveguide with varying grating corrugation depths δ_0. These simulations were performed using the commercial software ANSYS FDTD. The grating parameters are as follows: the grating period $\Lambda = 438$ nm, the apodization strength $b = 10$, the grating teeth number $N = 40$, and the number of resonators in cascade $N_p = 3$. Here, the small N_p is chosen to avoid computational complexity. The center width w_0 is fixed at 600 nm while δ_0 is varied from 400 to 700 nm, respectively. The apodized grating design achieves remarkably low propagation losses of 0.35, 0.72, 0.9, and 2.3 dB mm^{-1} for n_g of 3.4, 3.6, 4.0, and 4.2, respectively, indicating that the grating corrugation in the field-enhancement regions does not introduce significant excess losses (ELs). Although reducing the corrugation depth below 400 nm can further decrease the propagation loss and increase the optical bandwidth, it also lowers the group index and reduces the modulation efficiency. Figure 2d gives a comparison of the ELs between the proposed slow-light waveguide based on apodized gratings and the conventional structure (corresponding $b = 0$) used in [23] (more details about the conventional structure are shown in Note S2, Supporting Information). The conventional slow-light waveguide exhibits pretty high propagation losses up to 14, 20, and 25 dB mm^{-1} for group indices of 3.4, 3.8, and 4.1, respectively. In contrast, the excess loss of the present design with apodized gratings is reduced greatly by more than an order of magnitude compared to the conventional one. We notice the non-monotonic behavior in propagation loss as δ_0 increases. This arises from the scattering loss mechanism in the slow-light structure, as observed previously.[49] For the present structure, as n_g increases from 3.6 to 4.0, the grating corrugation depth δ_0 increases from 400 nm to 600 nm, which is still shallow and does not introduce strong light interaction with the sidewalls. As a result, the propagation loss increases slightly. In contrast, when $n_g > 4.0$, the grating corrugation depth δ_0 increases to 700 nm, and the optical field begins to interact notably with the grating sidewalls, thus exacerbating the scattering losses and leading to the observed jump in loss. Figure 2e shows the simulated light propagation in the present (left) and conventional (right) slow-light waveguides designed with $n_g \approx 4.2$, respectively. The apodized-grating design maintains low propagation losses even with enhanced n_g, while the conventional one suffers from significant optical attenuation.

The influences of the parameters such as N_p, N, δ_0, and w_0 on the ELs, the group index n_g, and the optical bandwidth BW_3dB are analyzed carefully. It can be seen from **Figure** 3a–c that n_g is insensitive to the resonator number N_p while the ELs increase slightly with the number N_p because of the increased

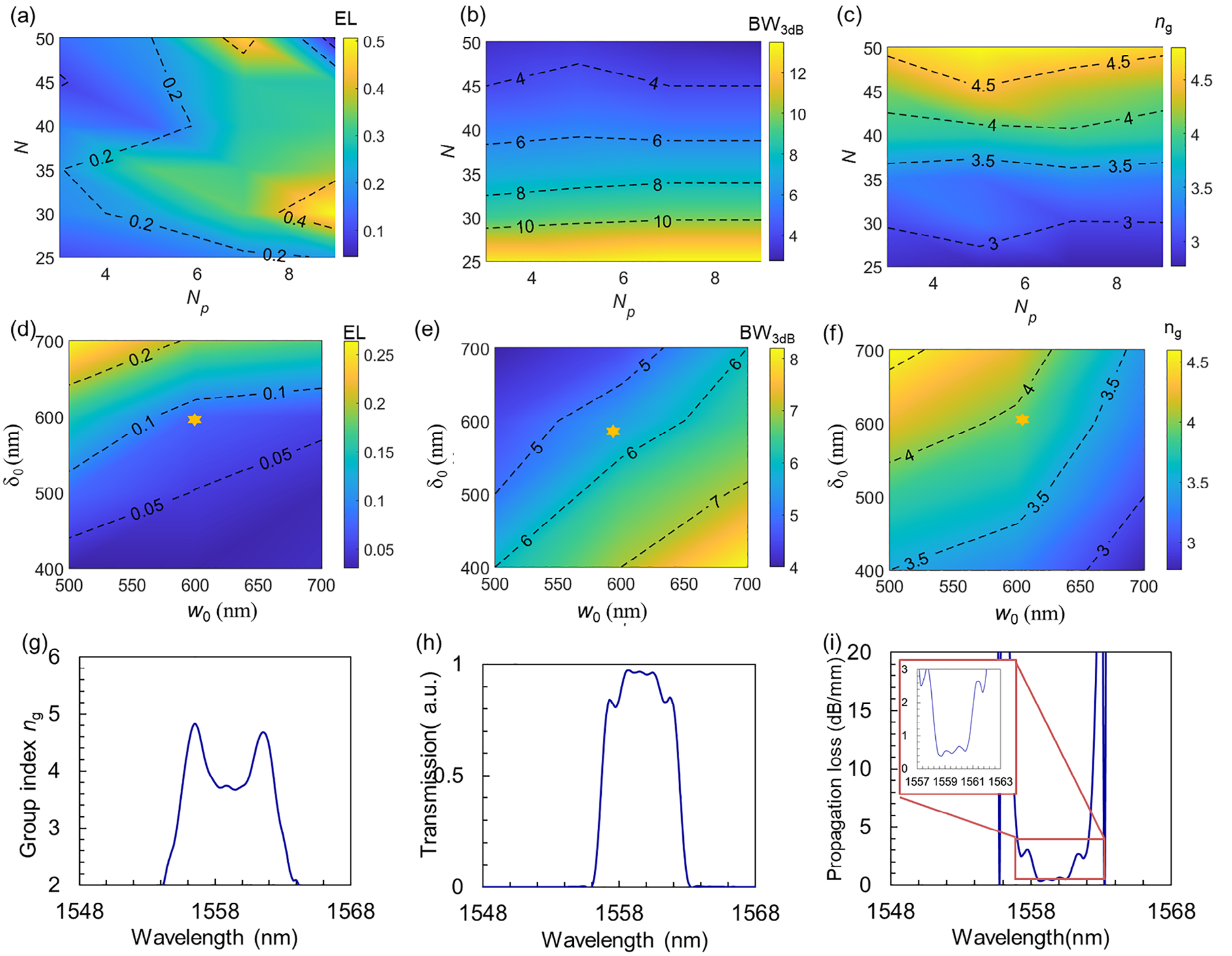

Figure 3. Simulated results for the slow-light structure with different structural parameters. a–c) are ELs, optical bandwidth $BW_{3\ dB}$, group index n_g, related to N_p and N, with $w_0 = 600$ nm and $\delta_0 = 0.6$ µm. d–f) are related to δ_0 and w_0 with $N_p = 5$ and $N = 40$. Calculated optimal apodized slow-light waveguide results: g) group index n_g. h) transmission spectrum. i) calculated propagation loss.

propagation length. When the grating period number N increases, the 3-dB optical bandwidth of the spectrum decreases while the group index increases gradually. It is seen that there is a trade-off between the modulation efficiency and the optical bandwidth. Moreover, as shown in Figure 3d–f, the slow-light effect can be enhanced with an increased refractive index n_g by increasing the corrugation depth δ_0 or decreasing the center width w_0 of the Bragg-grating resonators. On the other hand, the expense is that the $BW_{3\ dB}$ decreases. To balance the optical bandwidth and the modulation efficiency, the structural parameters are chosen as $\Lambda = 437$ nm, $w_0 = 0.6$ µm, $\delta_0 = 0.6$ µm, $N_p = 80$, and $N = 40$. Figure 3g–i shows the calculated results of the group index n_g, the transmission spectrum, and the corresponding propagation loss for the optimally designed slow-light waveguide, which gives an optical group refractive index n_g of ≈3.8 within a $BW_{3\ dB}$ more than 5.5 nm, with a minimum propagation loss of 0.3–0.6 dB mm^{-1}. It should be noted that there are some weak ripples on the top of the transmission spectrum, which may come from the wavelength dependence of the coupling coefficient. The ultralow-loss performance enables a 2.8-mm-long modulation region, which is impractical for conventional slow-light waveguides due to their prohibitively high ELs.

The MZM incorporates a ground-signal-ground (GSG) traveling-wave electrode configuration with CLTW (Figure 1d) to achieve velocity matching between the electrical and optical signals. T-shaped periodic structures are introduced between the ground and signal electrodes to minimize the electrode gap, maintain impedance matching, and reduce the electrical signal velocity. The electrode parameters are carefully designed following the procedure above to be (W_d, W_t, d, W_h, g, W_s) = (2, 46, 2, 20, 4.4, 25) µm. With these optimized parameters and 2.8-mm-long modulation length, the characteristic impedance, the RF effective index, and the RF loss α, EO response are calculated, as shown in **Figure 4**. Simulations indicate an electro-optic (EO) bandwidth exceeding 320 GHz for the 2.8-mm-long device. We also calculated the electro-optic response of a slow-light TFLN modulator using a general traveling-wave electrode with the same modulation length. Its 3 dB electro-optic

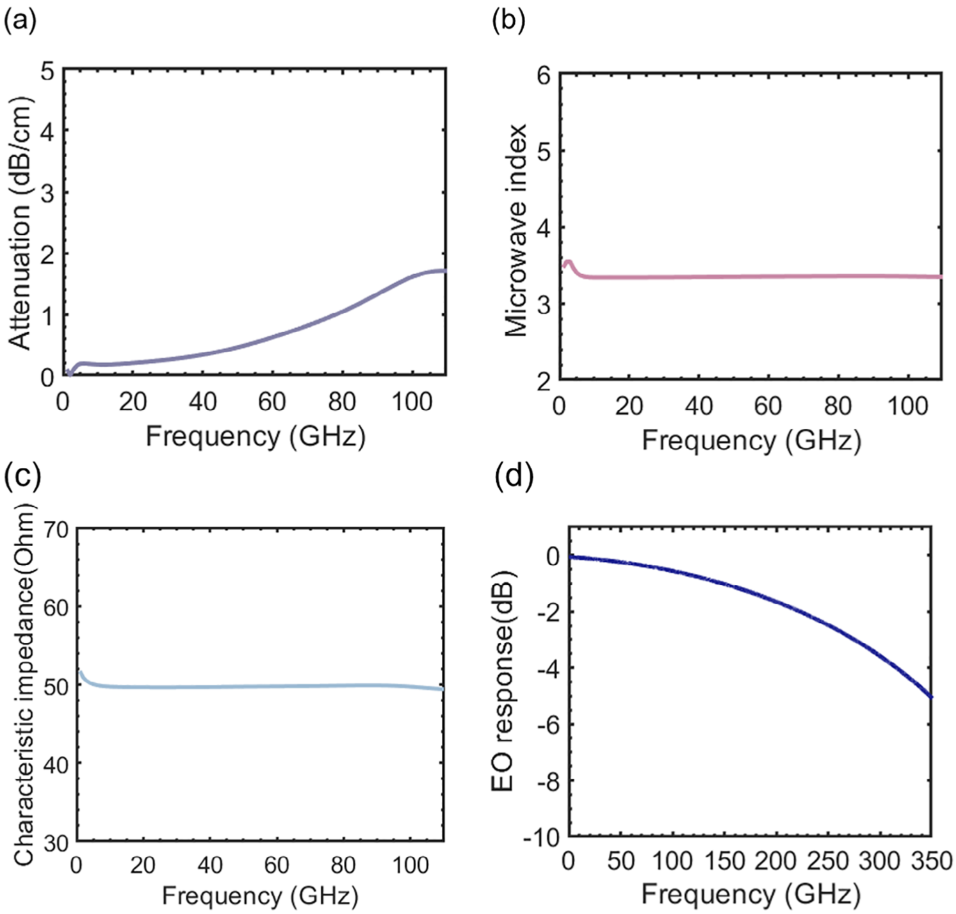

Figure 4. Calculated RF properties for the designed CLTW electrode, a) RF attenuation, b) RF effective index, c) characteristic impedance, d) calculated EO response.

bandwidth is ≈45 GHz, which is much smaller than that of the proposed capacitor-loaded electro-optic bandwidth (see Note S3, Supporting Information for more details).

Figure 5a–d shows the fabricated TFLN slow-light modulators (see more details about the fabrication in Note S4, Supporting Information). The apodized grating design, with reduced corrugation strength toward the resonator edges, eliminates the need for transition regions between the straight and slow-light waveguides (Figure 5d). The half-wave voltage measurements of the fabricated Mach-Zehnder modulator (MZM) were characterized by applying a 50-kHz triangular wave signal from an arbitrary function generator (AFG) and measuring the output with an oscilloscope (DSO) via a photodetector (PD) (Figure 5e). Sweeping the voltage from −4 to 4 V reveals a half-wave voltage (V_π) of 4.4 V, corresponding to a modulation efficiency ($V_\pi L$) of 1.23 V cm. The observed enhancement in $V_\pi L$ directly attributed to the enhancement of n_g, compared to conventional TFLN modulators (typically $V_\pi L = 2.2$ V with $n_g \approx 2.2$[15]). These results align with the theoretical framework of Equation (1), which establishes a linear dependence of $V_\pi\ L$ on n_g. Based on the measured results of $V_\pi L$, this fabricated slow-light waveguide has an enhanced group index n_g of ≈3.8, which agrees well with the calculated result in Figure 3. The optical properties of the slow-light waveguides are further investigated (Note S5, Supporting Information).

The measured 3-dB optical bandwidth is ≈6 nm (i.e., 1550.3–1556.6 nm) and remains insensitive to the number of cascaded resonators N_p. As the number of grating teeth N increases, the propagation loss remains nearly constant. At the same time, the slow-light effect is enhanced, and the optical bandwidth gradually reduces from 6 nm to 2 nm, consistent with previous reports.[39]

The propagation losses were normalized against a nearby straight waveguide to isolate the additional losses due to vertical coupling. Then, we quantified losses by extracting and fitting the slope of the relationship between length and loss in slow-light waveguides of varying lengths. Figure 5f shows the measured propagation losses for slow-light waveguides with N_p = 10, 50, and 80, as well as $N = 40$. The inset shows an image of the fabricated slow-light waveguides with different N_p. Remarkably, the present design achieves a low propagation loss of only ≈0.6 dB mm^{-1} using our laboratory's process, compared to the 2.0 dB cm^{-1} propagation loss of the fabricated straight waveguide using the same process. This is more than an order of magnitude lower than that of conventional slow-light waveguides.[23] The fabricated MZM achieves an ultra-low αV_πL of 7.4 dB V, making it the best-performing slow-light modulator reported to date.

Figure 6a shows the measured EO responses S_{21} of the fabricated MZM when operating at different operation wavelengths of 1550.5, 1553.5, and 1556.1 nm, respectively, using the

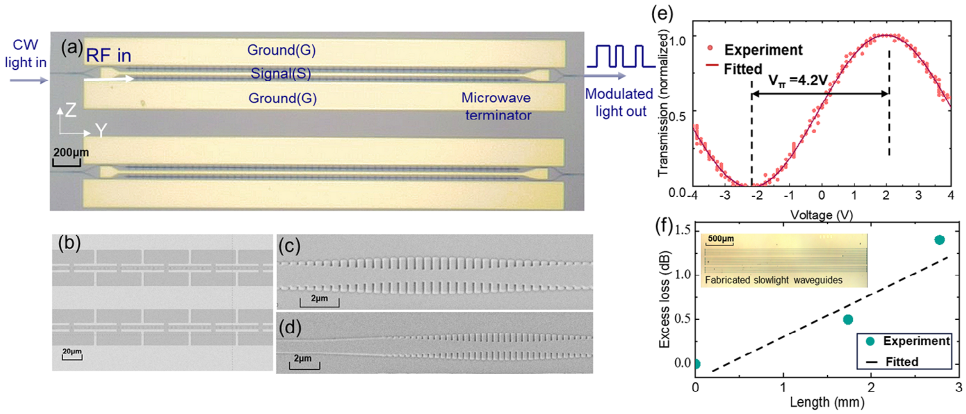

Figure 5. a) Optical microscope images of fabricated slow-light MZMs. Scanning electron microscopy pictures of the modulation section b), the apodized Bragg-grating c) and the waveguide junction between the regular waveguide and the slow-light waveguide d). e) Normalized optical transmissions of the fabricated LNOI photonic chip as a function of the applied voltage. f), Static extinction ratio (ER) as a function of the applied voltage. f) Measured propagation losses for waveguides with N_p = 10, 50, and 80.

experimental setup described in Note S4 (Supporting Information). The frequency range is limited to 67 GHz due to the Lightwave component analyzer (LCA) constraints. Notably, the EO responses remain flat without roll-off within the measured frequency range for all operating wavelengths spanning the 6-nm 3-dB optical bandwidth, which is in excellent agreement with theoretical predictions. The slow-light MZM is further evaluated for high-speed data transmission. Figure 6b–d shows the measured eye diagrams for 100 Gbps on-off keying (OOK), 200 Gbps four-level pulse amplitude modulation (PAM4), and 150 Gbps eight-level pulse amplitude modulation (PAM8) signals, all driven with a peak-to-peak voltage (V_{pp}) of 2.0 V. The eye diagrams exhibit wide openings and high extinction ratios of 4.5, 3.8, and 3.6 dB for the 100 Gbps OOK, 200 Gbps PAM4, and 150 Gbps PAM8 signals, respectively, confirming the modulator's excellent performance at high data rates. The energy efficiency of the slow-light MZM is estimated to be 40 fJ bit^{-1} for 200 Gbps PAM4 signaling. Remarkably, the power consumption can be further reduced by extending the modulation region length, leveraging the ultralow excess losses (ELs) of the slow-light waveguide design.

3. Discussion and Conclusion

In this work, we have proposed a novel approach to overcome the long-standing challenge of achieving low-loss, compact, and high-performance EO modulators by introducing novel apodized gratings in cascade for slow-light waveguides. The key advantage of the present design lies in its ultra-low propagation loss of 0.6 dB mm^{-1}, which is over an order of magnitude lower than conventional slow-light waveguides. The present slow-light waveguide with apodized gratings is allowed to directly connect to the input/output straight waveguides without any additional mode converters. In particular, the slow-light strategy enabling ultra-low losses allows to use of a relatively long modulation region (which is not achievable for conventional slow-light modu-

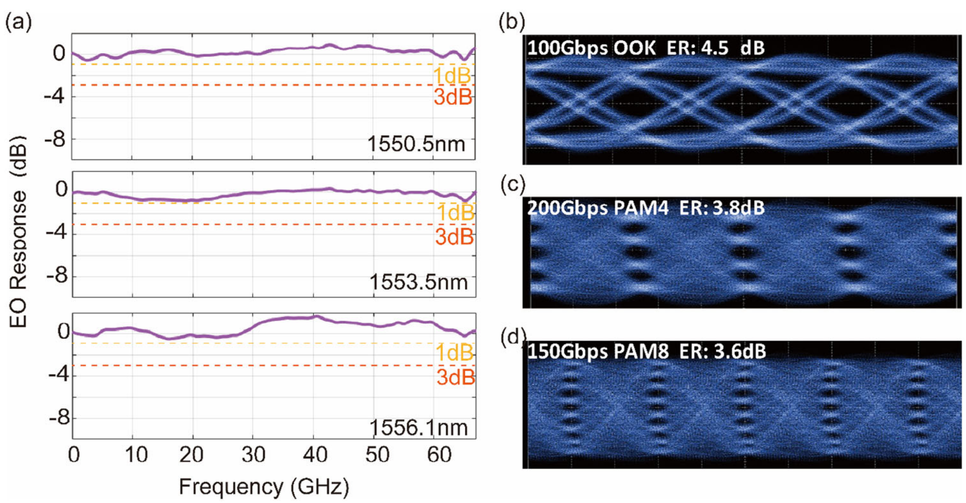

Figure 6. a) Measured EO responses for the fabricated slow-light modulator under different working wavelengths spanning from 1550.5 to 1556.1 nm. b–d) Measured optical eye-diagrams at data rates of 100 Gbps OOK, 200 Gbps PAM4, and 150 Gbps PAM8.

lators with high losses), which consequently helps to achieve improved dynamic ERs and lowered drive voltages, paving the way for high-performance EO modulators even supporting advanced modulation formats such as PAM-4 and PAM-8. The present slow-light MZM has a high modulation efficiency of 1.23 V cm, which is about twice higher than regular MZMs without slow-light structures. In addition, the periodic CLTW electrodes have been utilized to overcome the mismatch of the impedance and velocity for the electrical and optical signals, greatly enhancing the modulation bandwidth to be far beyond 67 GHz (the maximal bandwidth of the equipment).

The present slow-light MZM shows a broad optical bandwidth of 6 nm, which is sufficient for Lan-wavelength-division multiplexing (LWDM) with a channel spacing of 4.5 nm as well as DWDM with a narrow channel spacing of ≈0.8/1.6 nm or more. Compared with those EO modulators based on, e.g., microring resonators or photonic-crystal cavities, our design greatly relaxes the critical requirement for the operation-wavelength alignment and making the device robust to external environmental variations, thus reducing the power consumption for the resonance-wavelength control. Such compact and broadband phase modulation also provides a promising path to be scaled for WDM and coherent modulation techniques.

Table S1 (Supporting Information) gives a summary of the reported devices, including the loss-efficiency product $\alpha V_\pi L$, the data BR, the normalized ER, and the EO bandwidth. Clearly, silicon EO modulators still need to be improved regarding the high losses as well as the limited EO bandwidth, which thus hinders their use for satisfying the ever-increasing demand for ultra-high-BR data transmission. In contrast, TFLN EO modulators indeed provide a promising option with reduced losses and improved bandwidths, while the modulation efficiency is still low due to the limited EO coefficient of LN, and thus, centimeter-scale modulation regions are usually necessary for lowering the voltage V_{pp}. In contrast, 784 nm modulators (ref. [29]) attain enhanced modulation efficiency through reduced optical mode confinement, yet these attributes render them incompatible with telecommunication wavelengths. As demonstrated previously, with the assistance of slow-light structures, one can enhance the modulation efficiency and shrink the footprint for the EO modulators, which, however, still suffer from the issues related to high propagation losses, limited EO bandwidths, and narrow optical bandwidths.

As shown in Table S1 (Supporting Information), our fabricated TFLN slow-light modulator with optimized parameters has highlighted an ultra-low value of $\alpha V_\pi L$ (≈7.4 dB V) among the reported high-efficiency modulators, with low losses of 0.6 dB mm^{-1}, a high modulation efficiency $V_\pi L$ of 1.23 V cm, a compact footprint of ≈2.8 mm, low driving voltage (i.e., low power consumption) of 2 V, as well as high optical bandwidths of ≈6 nm simultaneously. Experimentally, we have obtained a flat EO response up to 67 GHz, while the calculated 3-dB EO bandwidth reaches 320 GHz, showing the great potential for ultra-high-speed data modulation. Here, data transmissions with 100 Gbps OOK, 200 Gbps PAM4, and 150 Gbps PAM8 signals with high ERs (4.5, 3.8, and 3.6 dB) have been demonstrated successfully, showcasing the great potential to work with advanced modulation formats. A higher bit rate beyond 200 Gbps is possible if an advanced experimental setup is available.

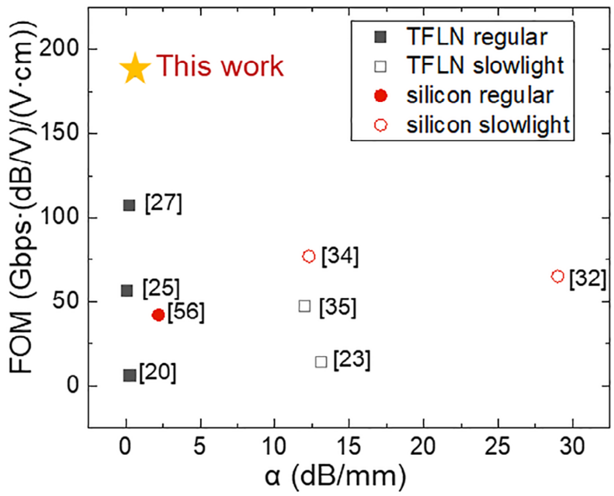

Figure 7. The FOM for TFLN and silicon MZMs reported. Here FOM = BR×(ER/V_{pp}) /(V_πL).

In order to give a comprehensive evaluation of the overall performance of high-speed optical modulators, here we define a special figure-of-merit (FOM) as the product of the bit rate (BR), the normalized extinction ratio (ER) and $1/(V_\pi L)$, i.e., FOM = BR×(ER/V_{pp})/($V_\pi L$). A higher FOM is obtained for an optical modulator with a higher BR, a higher normalized ER as well as a lower $V_\pi L$ (higher modulation efficiency). **Figure 7** shows the calculated FOM for all the optical modulators reported. As it can be seen, the FOM of the most reported optical modulator is no more than 100. One of the representative slow-light silicon modulators is the one reported with 110 GHz in,[32] which has a loss as high as 29.8 dB mm^{-1} and an FOM of 65 Gbps•(dB/V)/(V•cm). Another example is the slow-light TFLN modulator reported in,[23] showing a loss of 13.3 dB mm^{-1} and a FOM of 14 Gbps•(dB/V)/(V•cm). In contrast, the present slow-light modulator works with a low loss of 0.6 dB/mm and a FOM as high as 182 Gbps•(dB/V)/(V•cm), which is a new record. From the comparison given in Figure 7 and Table S1 (Supporting Information), it can be seen that the present slow-light modulator is an example with the best overall performance to satisfy the demands of real applications. It is worth noting that ref. [15] reports a high-performance modulator with favorable values with low waveguide loss and 210 Gbps data transmission. However, as the dynamic extinction ratio under specified drive conditions is not explicitly reported, a reliable FOM value cannot be extracted for inclusion in Figure 7.

Further reducing the device loss is possible when using standard UV lithography (instead of the E-beam lithography used here) because the stitching errors and the sidewall roughness can be minimized. The feasibility of UV lithography for fabricating sub-wavelength structures has been well-established through industry-scale implementations,[55] which is helpful for the fabrication of sub-wavelength photonic structures.

Improving the dynamic ER for higher-order modulation formats can be addressed through electronic and photonic equalization techniques.[56–58] Finally, co-integration with laser sources and coherent receiver circuitry will be very attractive for the deployment of next-generation optical communication systems.

In summary, this groundbreaking slow-light modulator has been developed to overcome the trade-offs between the optical loss, the device size, the modulation efficiency, and the bandwidth that have hindered conventional EO modulators. By offering a new route to high-density, energy-efficient, and ultra-high-speed optical interconnects, our approach opens the door to Terabit/s-scale datacom and computation applications.

Supporting Information

Supporting Information is available from the Wiley Online Library or from the author.

Acknowledgements

This work was funded in part by National Natural Science Foundation of China (NSFC) (62405271, 62205286, 92150302, U23B2047, 62321166651), China Postdoctoral Science Foundation (2023M733039), Natural Science Foundation of Zhejiang Province (LQ21F050006), the Innovation Program for Quantum Science and Technology (2021ZD0301500).

Conflict of Interest

The authors declare no conflict of interest.

Data Availability Statement

The data that support the findings of this study are available from the corresponding author upon reasonable request.

Keywords

electro-optic, lithium niobate, loss, modulator, slow light

Received: November 22, 2024
Revised: May 13, 2025
Published online:

[1] Q. Cheng, M. Bahadori, M. Glick, S. Rumley, K. Bergman, *Optica* **2018**, *5*, 1354.
[2] S. Shekhar, W. Bogaerts, L. Chrostowski, J. E. Bowers, M. Hochberg, R. Soref, B. J. Shastri, *Nat. Commun.* **2024**, *15*, 751.
[3] R. Guo, M. Decker, F. Setzpfandt, X. Gai, D.-Y. Choi, R. Kiselev, A. Chipouline, I. Staude, T. Pertsch, D. N. Neshev, *Sci. Adv.* **2017**, *3*, 1700007.
[4] A. Rizzo, A. Novick, V. Gopal, B. Y. Kim, X. Ji, S. Daudlin, Y. Okawachi, Q. Cheng, M. Lipson, A. L. Gaeta, K. Bergman, *Nat. Photonics* **2023**, *17*, 781.
[5] S. Fathololoumi, C. Malouin, D. Hui, K. Al-Hemyari, K. Nguyen, P. Seddighian, Y.-J. Chen, Y. Wang, A. Yan, R. Defrees, 2022 IEEE Symposium on High-Performance Interconnects (HOTI), **2022**.
[6] I. Taghavi, M. Moridsadat, A. Tofini, S. Raza, N. A. Jaeger, L. Chrostowski, B. J. Shastri, S. Shekhar, *Nanophotonics* **2022**, *11*, 3855.
[7] J. Sun, R. Kumar, M. Sakib, J. B. Driscoll, H. Jayatilleka, H. Rong, *J. Lightwave Technol.* **2018**, *37*, 110.
[8] M. Eppenberger, A. Messner, B. I. Bitachon, W. Heni, T. Blatter, P. Habegger, M. Destraz, E. De Leo, N. Meier, N. Del Medico, C. Hoessbacher, B. Baeuerle, J. Leuthold, *Nat. Photonics* **2023**, *17*, 360.
[9] B. Murray, C. Antony, G. Talli, P. D. Townsend, *IEEE Photonics J.* **2022**, *14*, 7220611.
[10] M. Ayata, Y. Fedoryshyn, W. Heni, B. Baeuerle, A. Josten, M. Zahner, U. Koch, Y. Salamin, C. Hoessbacher, C. Haffner, *Science* **2017**, *358*, 630.
[11] A. Liu, R. Jones, L. Liao, D. Samara-Rubio, D. Rubin, O. Cohen, R. Nicolaescu, M. Paniccia, *Nature* **2004**, *427*, 615.
[12] J. Liu, M. Beals, A. Pomerene, S. Bernardis, R. Sun, J. Cheng, L. C. Kimerling, J. Michel, *Nat. Photonics* **2008**, *2*, 433.
[13] M. Lee, H. E. Katz, C. Erben, D. M. Gill, P. Gopalan, J. D. Heber, D. J. McGee, *Science* **2002**, *298*, 1401.
[14] C. Haffner, D. Chelladurai, Y. Fedoryshyn, A. Josten, B. Baeuerle, W. Heni, T. Watanabe, T. Cui, B. Cheng, S. Saha, *Nature* **2018**, *556*, 483.
[15] C. Wang, M. Zhang, X. Chen, M. Bertrand, A. Shams-Ansari, S. Chandrasekhar, P. Winzer, M. Loncar, *Nature* **2018**, *562*, 101.
[16] M. Xu, Y. Zhu, F. Pittalà, J. Tang, M. He, W. C. Ng, J. Wang, Z. Ruan, X. Tang, M. Kuschnerov, L. Liu, S. Yu, B. Zheng, X. Cai, *Optica* **2022**, *9*, 61.
[17] Y. Xue, R. Gan, K. Chen, G. Chen, Z. Ruan, J. Zhang, J. Liu, D. Dai, C. Guo, L. Liu, *Optica* **2022**, *9*, 1131.
[18] B. C. Pan, L. H. Xuan, X. Hao-Chen, H. Y. Shu, L. Huan, Y. Z. Jie, L. Liu, S. Y. Cheng, D. D. Xin, *Chip* **2022**, *1*, 100029.
[19] P. Kharel, C. Reimer, K. Luke, L. He, M. Zhang, *Optica* **2021**, *8*, 357.
[20] C. Wang, M. Zhang, B. Stern, M. Lipson, M. Loncar, *Opt. Express* **2018**, *26*, 1547.
[21] M. Li, J. Ling, Y. He, U. A. Javid, S. Xue, Q. Lin, *Nat. Commun.* **2020**, *11*, 4123.
[22] B. Pan, H. Cao, Y. Huang, Z. Wang, K. Chen, H. Li, Z. Yu, D. Dai, *Photonics Res.* **2022**, *10*, 697.
[23] G. Chen, H. Wang, B. Chen, Z. Ruan, C. Guo, K. Chen, L. Liu, *Nanophotonics* **2023**, *12*, 3603.
[24] A. Boes, L. Chang, C. Langrock, M. Yu, M. Zhang, Q. Lin, M. Loncar, M. Fejer, J. Bowers, A. Mitchell, *Science* **2023**, *379*, abj4396.
[25] M. He, M. Xu, Y. Ren, J. Jian, Z. Ruan, Y. Xu, S. Gao, S. Sun, X. Wen, L. Zhou, *Nat. Photonics* **2019**, *13*, 359.
[26] M. Xu, W. Chen, M. He, X. Wen, Z. Ruan, J. Xu, L. Chen, L. Liu, S. Yu, X. Cai, *APL Photonics* **2019**, *4*, 100802.
[27] Z. Wang, G. Chen, Z. Ruan, R. Gan, P. Huang, Z. Zheng, L. Lu, J. Li, C. Guo, K. Chen, L. Liu, *ACS Photonics* **2022**, *9*, 2668.
[28] Z. Yu, D. Tu, W. Yan, H. Guan, L. Jiang, X. Sun, Z. Li, *IEEE Photonics J.* **2024**, *16*, 9900075.
[29] F. Valdez, V. Mere, S. Mookherjea, *Optica* **2023**, *10*, 578.
[30] Y. Enami, C. T. Derose, D. Mathine, C. Loychik, C. Greenlee, R. A. Norwood, T. D. Kim, J. Luo, Y. Tian, A. K. Y. Jen, N. Peyghambarian, *Nat. Photonics* **2007**, *1*, 180.
[31] Y. Zhang, J. Shen, J. Li, H. Wang, C. Feng, L. Zhang, L. Sun, J. Xu, M. Liu, Y. Wang, *Light: Sci. Appl.* **2023**, *12*, 206.
[32] C. Han, Z. Zheng, H. Shu, M. Jin, J. Qin, R. Chen, Y. Tao, B. Shen, B. Bai, F. Yang, Y. Wang, H. Wang, F. Wang, Z. Zhang, S. Yu, C. Peng, X. Wang, *Sci. Adv.* **2023**, *9*, adi5339.
[33] C. Deng, L. Zhu, M. Lu, Y. Sun, L. Huang, D. Wang, G. Hu, B. Yun, Y. Cui, *Opt. Laser Technol.* **2023**, *158*, 108769.
[34] O. Jafari, W. Shi, S. Larochelle, *IEEE Photonics Technol. Lett.* **2020**, *32*, 445.
[35] X. Huang, Y. Liu, H. Guan, Z. Yu, M. Tan, Z. Li, *IEEE Photonics Technol. Lett.* **2021**, *33*, 1093.
[36] X. Huang, Y. Liu, H. Guan, Z. Yu, M. Tan, Z. Li, *IEEE Photonics J.* **2021**, *13*, 6600305.
[37] R. W. Boyd, D. J. Gauthier, *Science* **2009**, *326*, 1074.
[38] M. O. Scully, M. S. Zubairy, *Science* **2003**, *301*, 181.
[39] T. F. Krauss, *Nat. Photonics* **2008**, *2*, 448.

[40] u. A. Vlasov, M. O'Boyle, H. F. Hamann, S. J. McNab, *Nature* **2005**, *438*, 65.
[41] T. Baba, *Nat. Photonics* **2008**, *2*, 465.
[42] J. Shen, Y. Zhang, L. Zhang, J. Li, C. Feng, Y. Jiang, H. Wang, X. Li, Y. He, X. Ji, *Laser Photo. Rev.* **2024**, 2401092.
[43] A. Yariv, Y. Xu, R. K. Lee, A. Scherer, *Opt. Lett.* **1999**, *24*, 711.
[44] J. K. Poon, J. Scheuer, Y. Xu, A. Yariv, *JOSA B* **2004**, *21*, 1665.
[45] S. Hughes, L. Ramunno, J. F. Young, J. Sipe, *Phys. Rev. Lett.* **2005**, *94*, 033903.
[46] S. Hughes, L. Ramunno, J. F. Young, J. J. P. r. l. Sipe, *Phys. Rev. Lett.* **2005**, *94*, 033903.
[47] E. Kuramochi, M. Notomi, S. Hughes, A. Shinya, T. Watanabe, L. Ramunno, *Phys. Rev. B* **2005**, *72*, 161318.
[48] H. Takesue, N. Matsuda, E. Kuramochi, W. J. Munro, M. Notomi, *Nat. Commun.* **2013**, *4*, 2725.
[49] S. A. S. L. O'Faolain, D. M. Beggs, T. P. White, M. Spasenović, L. Kuipers, F. Morichetti, A. Melloni, S. Mazoyer, J. P. Hugonin, P. Lalanne, T. F. Krauss, *Opt. Exp.* **2010**, *18*, 27627.
[50] M. Notomi, E. Kuramochi, T. Tanabe, *Nat. Photonics* **2008**, *2*, 741.
[51] J. He, D. Liu, B. Pan, Y. Huang, M. Zhu, M. Zhang, D. Dai, *Opt. Express* **2022**, *30*, 34140.
[52] B. Gul, F. Ahmad, IoT and Analytics for Sensor Networks: Proceedings of ICWSNUCA **2021**.
[53] X. Gao, L. Yang, H. Lin, L. Zhang, J. Li, F. Bo, Z. Wang, L. Lu, *Nat. Nanotechnol.* **2020**, *15*, 1012.
[54] L. Zhang, L. Jie, M. Zhang, Y. Wang, Y. Xie, Y. Shi, D. Dai, *Photonics Res.* **2020**, *8*, 684.
[55] K. Giewont, S. Hu, B. Peng, M. Rakowski, S. Rauch, J. C. Rosenberg, A. Sahin, I. Stobert, A. Stricker, K. Nummy, F. A. Anderson, J. Ayala, T. Barwicz, Y. Bian, K. K. Dezfulian, D. M. Gill, T. Houghton, *IEEE J. Sel. Top. Quantum Electron.* **2019**, *25*, 8200611.
[56] J. Lin, H. Sepehrian, L. A. Rusch, W. Shi, *Opt. Express* **2019**, *27*, 5610.
[57] M. Li, L. Wang, X. Li, X. Xiao, S. Yu, *Photo. Res.* **2018**, *6*, 109.
[58] Y. Zhu, F. Zhang, F. Yang, L. Zhang, X. Ruan, Y. Li, Z. Chen, *J. Lightwave Technol.* **2020**, *38*, 67.